| Title | **Single-ensemble-based eigen-processing methods for color flow imaging-Part II. the matrix pencil estimator** |
|---|---|
| Author(s) | **Yu, ACH; Cobbold, RSC** |
| Citation | **Ieee Transactions On Ultrasonics, Ferroelectrics, And Frequency Control, 2008, v. 55 n. 3, p. 573-587** |
| Issued Date | **2008** |
| URL | **http://hdl.handle.net/10722/57477** |
| Rights | **Creative Commons: Attribution 3.0 Hong Kong License** |

# Single-Ensemble-Based Eigen-Processing Methods for Color Flow Imaging—Part II. The Matrix Pencil Estimator

Alfred C. H. Yu, *Member, IEEE*, and Richard S. C. Cobbold, *Life Member, IEEE*

*Abstract*—Parametric spectral estimators can potentially be used to obtain flow estimates directly from raw slow-time ensembles whose clutter has not been suppressed. We present a new eigen-based parametric flow estimation method called the matrix pencil, whose principles are based on a matrix form under the same name. The presented method models the slow-time signal as a sum of dominant complex sinusoids in the slow-time ensemble, and it computes the principal Doppler frequencies by using a generalized eigenvalue problem formulation and matrix rank reduction principles. Both fixed-rank (rank-one, rank-two) and adaptive-rank matrix pencil flow estimators are proposed, and their potential applicability to color flow signal processing is discussed. For the adaptive-rank estimator, the nominal rank was defined as the minimum eigen-structure rank that yields principal frequency estimates with a spread greater than a prescribed bandwidth. In our initial performance evaluation, the fixed-rank matrix pencil estimators were applied to raw color flow data (transmit frequency: 5 MHz; pulse repetition period: 0.175 ms; ensemble size: 14) acquired from a steady flow phantom (70 cm/s at centerline) that was surrounded by rigid-tissue-mimicking material. These fixed-rank estimators produced velocity maps that are well correlated with the theoretical flow profile (correlation coefficient: 0.964 to 0.975). To facilitate further evaluation, the matrix pencil estimators were applied to synthetic slow-time data (transmit frequency: 5 MHz; pulse repetition period: 1.0 ms; ensemble size: 10) modeling flow scenarios without and with tissue motion (up to 1 cm/s). The bias and root-mean-squared error of the estimators were computed as a function of blood-signal-to-noise ratio and blood velocity. The matrix pencil flow estimators showed that they are comparatively less biased than most of the existing frequency-based flow estimators like the lag-one autocorrelator.

## I. Introduction

IN ultrasound color flow imaging, estimation of the mean or modal flow velocity over a sample volume (or map pixel location) is often performed after the clutter in the slow-time signal has been adequately suppressed. As such, many forms of flow estimators are derived under the assumption that the slow-time signal only comprises echoes originating from moving blood scatterers and a filtered

form of background white noise. Perhaps the most well known of these estimators is the lag-one autocorrelator that computes the mean velocity by estimating the mean Doppler frequency from the lag-one autocorrelation value of the slow-time signal [1], [2]. Alternatively, some studies have proposed other forms of flow estimators like the time-domain cross-correlator [3] and the maximum likelihood estimator [4], [5] that are based on target-tracking principles. The potential drawback of these estimators is that their performance inherently depends on the clutter filter's ability to suppress slow-time clutter without distorting the blood echoes. In particular, estimation biases can be expected whenever the clutter filter distorts parts of the blood signal or fails to suppress clutter adequately. Moreover, at low blood-signal-to-noise ratios (BSNR), further estimation biases can be anticipated because the filtered white noise (i.e., colored noise) becomes more significant, and its presence can add further bias to the flow estimates.

### A. Review of Existing Parametric Flow Estimators

To account for the biasing effect of the clutter filter properly, it may be advantageous to use estimation strategies that can be directly applied to the raw (i.e., unfiltered) slow-time signal. This rationale may have motivated the development of parametric estimators that work by analyzing the principal Doppler spectral contents (i.e., they are frequency-based estimators). For example, Ahn and Park [6] have applied the autoregressive (AR) modeling method to extract both the principal clutter and blood Doppler frequencies simultaneously from the raw slow-time signal. As reviewed by Vaitkus and Cobbold [7], this approach works by computing the least-squares fit of a regressive signal model onto the raw slow-time data and solving for the characteristic spectral modes of the resulting model. However, as pointed out elsewhere [8], since the least-squares fitting procedure assumes that the slow-time data samples are free of noise perturbations, the accuracy of the AR modeling method tends to degrade significantly at low BSNR levels.

Another way of performing parametric spectral estimation is to make use of eigen-analysis principles. In particular, Allam and Greenleaf [9] have suggested that a form of eigen-analysis called multiple signal classification (MUSIC) can be used to obtain flow estimates without the prior use of clutter filters. Like the eigen-filter men-

tioned in [10], the MUSIC approach begins by computing the eigen-decomposition of the slow-time correlation matrix found from averaging multiple slow-time ensembles. It then solves for the principal Doppler frequencies by finding the spectral modes in a pseudospectrum defined from the reciprocal of the cross-correlation between noise eigen-components and various complex sinusoids (the two are orthogonal when the complex sinusoid frequency matches any of the signal eigen-components). Such an eigen-based formulation has also been adopted by Vaitkus and Cobbold [11], who proposed the use of a closed-form parametric estimator called Root-MUSIC to estimate principal flow velocities from raw slow-time data. Their approach, which uses a rank-two eigenstructure to model the raw slow-time signal, has been analyzed using in vivo color flow imaging data whose clutter can be sufficiently modeled as a single complex sinusoid [12].

### B. Motivations of Study

From the previous work on AR modeling and MUSIC, it can be seen that parametric estimation strategies have potential in obtaining modal flow estimates in the presence of clutter. However, these parametric estimators have individual limitations that reduce their efficacy in color flow data processing. In particular, as noted earlier, the least-squares fitting procedure used by an AR estimator to perform the model regression is only effective at high BSNR. As for MUSIC, its multi-ensemble averaging approach to the estimation of the slow-time correlation matrix inherently requires statistical stationarity among the slow-time ensembles over the specified range of depth, and such approach is not always valid due to the spatially varying nature of tissue and flow dynamics.

In this paper, we present a principal spectral component estimator called the Matrix Pencil that is designed to work with each slow-time ensemble individually and describe how it can be used for flow estimation. This estimator works by exploiting the properties of an algebraic form known as matrix pencil and in turn treating flow estimation as a generalized eigenvalue (GE) problem. Its resilience against background white noise is achieved by making use of matrix rank reduction principles. To formulate discussion on the matrix pencil, the rest of the paper is organized as follows. The next section first provides a theoretical description of the matrix pencil estimation framework. Section III then discusses how this parametric spectral estimator can be applied to color flow signal processing. An in vitro case study aimed to facilitate initial assessment of the matrix pencil method is described in Section IV. Further analysis results based on the use of a simulation approach are described in Sections V and VI. Highlights of the matrix pencil method are summarized in Section VII.

## II. PRINCIPLES OF THE MATRIX PENCIL METHOD

Because it is a parametric spectral estimator, the matrix pencil method is based on the modeling of the raw slow-time signal as a summation of principal complex sinusoids. In particular, it is intended to work with a principal-component signal model given by:

$$\mathbf{x} = [x(0), x(1), \ldots, x(N_D - 1)]^T$$
$$= \mathbf{b} + \mathbf{c} + \mathbf{w} \approx \sum_{k=1}^{K} \chi_k \mathbf{v}_{\mathrm{CS}(k)} + \mathbf{w}. \qquad (1a)$$

In this equation, $x(n)$ is the $n$th sample in a raw slow-time ensemble, while $\mathbf{x}$, $\mathbf{b}$, $\mathbf{c}$, and $\mathbf{w}$, respectively, denote the data ensemble (consisting of $N_D$ samples) for raw slow-time signal, blood echoes, clutter, and white noise; also, $K$ is the number of principal components in the signal model, while $\chi_k$ denotes the weight of the $k$th complex sinusoid vector $\mathbf{v}_{\mathrm{CS}(k)}$. Note that $\mathbf{v}_{\mathrm{CS}(k)}$ can be expressed in the following vector form:

$$\mathbf{v}_{\mathrm{CS}(k)} = \left[1, z_k, z_k^2, \ldots, z_k^{(N_D-1)}\right]^T \text{ for } z_k = e^{j2\pi f_{\mathrm{D},k} T_{\mathrm{PRI}}}, \qquad (1b)$$

where $f_{\mathrm{D},k}$ is the $k$th principal Doppler frequency and $T_{\mathrm{PRI}}$ is the pulse repetition interval (i.e., the slow-time sampling period). It should be pointed out that, from a subspace perspective, this principal-component signal model is equivalent to the eigen-structure of a raw slow-time signal whose rank is equal to $K$.

### A. Basic Principles

In terms of its principles, the matrix pencil approach is primarily based on the solution to the following generalized eigenvalue (GE) problem:

$$\mathbf{A}_1 \mathbf{q} = \lambda \mathbf{A}_0 \mathbf{q} \iff (\mathbf{A}_1 - \lambda \mathbf{A}_0)\mathbf{q} = \mathbf{0}, \qquad (2)$$

where $\mathbf{A}_1$ and $\mathbf{A}_0$ are singular matrices of the same dimension and $\mathbf{q}$ is the generalized eigenvector for a particular eigenvalue $\lambda$. Note that the set of matrices $\mathbf{A}_1 - \lambda \mathbf{A}_0$ created from all values of $\lambda$ is known in linear algebra as a *matrix pencil*[1]. The GEs of $\mathbf{A}_1 - \lambda \mathbf{A}_0$ are the particular values of $\lambda$ that yield non-zero solutions to the eigenvector $\mathbf{q}$. Such values can also be regarded as those that reduce the matrix rank of $\mathbf{A}_1 - \lambda \mathbf{A}_0$ so that a non-empty nullspace exists.

Fig. 1 summarizes the overall formulation of the matrix pencil estimator, whose goal is to define $\mathbf{A}_1 - \lambda \mathbf{A}_0$ in such a way that their corresponding GEs can be used to find the principal slow-time frequencies. As described by Hua and Sarkar [13], one particular way to define this quantity is to set $\mathbf{A}_1$ and $\mathbf{A}_0$ as lag-one subsets of a Hankel data matrix $\mathbf{A}$. Specifically, for a slow-time ensemble size $N_D$, the matrix pair $[\mathbf{A}_1, \mathbf{A}_0]$ can be defined as follows:

---

[1]In mathematics, the term *pencil* generally refers to a set of entities that share a common property, such as passage through the same given point.
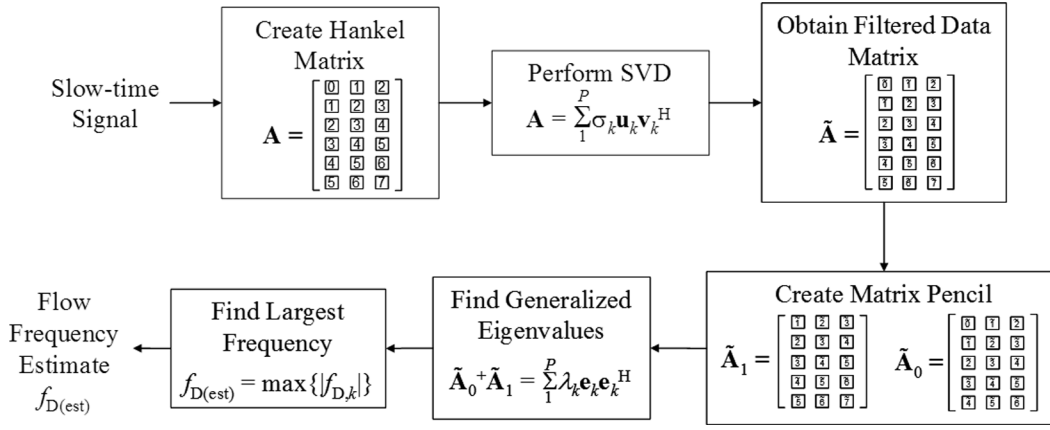
Fig. 1. Block diagram of the matrix pencil estimator involving matrix rank reduction. During operation, this estimator is applied to the slow-time signal of each sample volume.
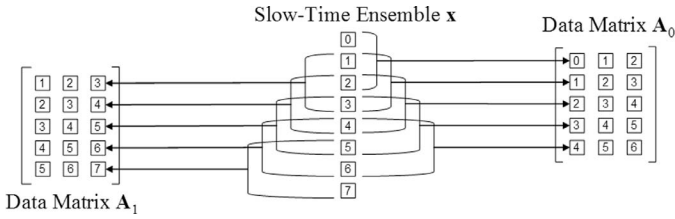


Fig. 2. Illustrating how the data matrices $\mathbf{A}_1$ and $\mathbf{A}_0$ are formed in the matrix pencil estimator for the case where $N_D = 8$ and $P = 3$.

$\mathbf{A} =$

$$\begin{bmatrix} x(0) & x(1) & \cdots & x(P-1) \\ x(1) & x(2) & \cdots & x(P) \\ \vdots & \vdots & \ddots & \vdots \\ x(N_D-P) & x(N_D-P+1) & \cdots & x(N_D-1) \end{bmatrix}_{(N_D-P+1)\times P}, \quad (3a)$$

$$\mathbf{A}_1 = \text{last } (N_D - P) \text{ rows of } \mathbf{A}, \quad (3b)$$

$$\mathbf{A}_0 = \text{first } (N_D - P) \text{ rows of } \mathbf{A}. \quad (3c)$$

An example on the construction of this matrix pair is given in Fig. 2. It is worth pointing out that, in $\mathbf{A}_1$ and $\mathbf{A}_0$, $P$ is a pencil dimension parameter that is similar to the one defined for the Hankel data matrix given in (2) of [10]. For a $K$th-order signal eigen-structure, this parameter must be set greater than $K$ but less than $\text{ceil}(N_D/2)$ (i.e., the smallest integer greater than or equal to $N_D/2$).

### B. Matrix Rank Reduction

As shown in Appendix A for the case without noise, the $K$ nonspurious GEs of the matrix pencil $\mathbf{A}_1 - \lambda\mathbf{A}_0$ defined via (3b) and (3c) essentially correspond to the signal modes $z_k$ of the principal-component signal model shown in (1). However, since noise is generally present in the acquired slow-time data, rank reduction needs to be performed on the matrix pair $[\mathbf{A}_1, \mathbf{A}_0]$ prior to the computation of the GEs. The rank reduction can essentially be carried out by using singular value decomposition (SVD) to create $\mathbf{A}_1$ and $\mathbf{A}_0$ from only their $K$ largest singular

components [13]. This approach is equivalent to a total-least-squares formulation of the estimation problem from a data fitting perspective [14]. Note that an efficient way of achieving rank reduction is to first compute the rank-reduced equivalent of $\mathbf{A}$ and then create the matrix pair from lag-one subsets of the rank-reduced matrix [15]. The rank-reduced data matrix $\tilde{\mathbf{A}}$ (assumed to be rank-$K$) and its corresponding matrix pair $[\tilde{\mathbf{A}}_1, \tilde{\mathbf{A}}_0]$ can be expressed as follows:

$$\tilde{\mathbf{A}} = \sum_{k=1}^{K} \sigma_k \mathbf{u}_k \mathbf{v}_k^H, \quad (4a)$$

$$\tilde{\mathbf{A}}_1 = \text{last } (N_D - P) \text{ rows of } \tilde{\mathbf{A}}, \quad (4b)$$

$$\tilde{\mathbf{A}}_0 = \text{first } (N_D - P) \text{ rows of } \tilde{\mathbf{A}}, \quad (4c)$$

where $\sigma_k$, $\mathbf{u}_k$, and $\mathbf{v}_k$ are, respectively, the singular value, left singular vector (of size $N_D - P + 1$), and right singular vector (of size $P$) for the $k$th SVD component of $\mathbf{A}$. It should be pointed out that the efficacy of rank reduction improves in general when there is a large difference between the signal eigen-rank $K$ and the matrix dimension parameter $P$.

### C. Computation of Principal Frequencies

As shown in Appendix A, the GEs of the matrix pair $[\mathbf{A}_1, \mathbf{A}_0]$ (or $[\tilde{\mathbf{A}}_1, \tilde{\mathbf{A}}_0]$) can be found from the eigenvalues of $\mathbf{A}_0^+ \mathbf{A}_1$ (or $\tilde{\mathbf{A}}_0^+ \tilde{\mathbf{A}}_1$), where the '+' superscript denotes a matrix's pseudoinverse (i.e., the singular matrix equivalent of a matrix inverse). Once the GEs are found, the $K$ principal Doppler frequencies can be calculated from the phase of the GEs as follows:

$$f_{D,k} = \frac{1}{2\pi T_{\text{PRI}}} \arg\{\lambda_k\}. \quad (5a)$$

Subsequently, the frequency estimates can be classified as to whether they correspond to clutter or blood echoes. An intuitive approach to perform this classification is to make use of the fact that blood echoes generally give rise to higher Doppler frequencies. As such, it is possible to

TABLE I
THREE TYPES OF MATRIX PENCIL ESTIMATORS FOR COLOR-FLOW DATA PROCESSING.

| Type | Principal | Main Use | Limitation |
|---|---|---|---|
| Rank-One $(K = 1)$ | Obtain one principal frequency estimate from a data ensemble | Find mode frequency of filtered slow-time data | Cannot be applied directly to raw slow-time data to estimate flow |
| Rank-Two $(K = 2)$ | Extract two principal frequencies from a data ensemble | Find modal flow estimates in presence of narrowband clutter | Estimates may be biased when applied to data with wideband clutter |
| Rank-Adaptive $(K = K_{\mathrm{nom}})$ | Compute principal frequencies using an eigen-rank found from spectral spread analysis | Find modal flow estimates in presence of any type of clutter | Assume clutter spans a prescribed bandwidth |

identify the modal blood Doppler frequency as follows from the principal spectral estimate with the largest magnitude:

$$f_{\mathrm{D(est)}} = f_{\mathrm{D},k_b} \text{ for } k_b = \arg\max_k \left\{ |f_{\mathrm{D},k}| \, \forall k \in [1, k] \right\}, \quad (5b)$$

which can then be converted into a velocity value via the Doppler equation.

### D. Relationship to Existing Eigen-Based Estimators

Following the same derivation given in Section II-C of [10], it can be seen that the matrix pencil is similar to the data-smoothed version of an eigen-decomposition-based spectral estimator that involves the computation of GEs for a rank-reduced matrix pair defined from the $K$ largest eigen-components. As described by Stoica and Soderstrom [16], such an eigen-decomposition equivalent of the matrix pencil can be considered as a data-smoothed form of an eigen-processing strategy called "estimation of signal parameters via rotational invariance techniques" (ESPRIT) [17]. It is worth pointing out that, besides data-smoothed ESPRIT, a data-smoothed version of MUSIC also exists in practice [16]. In color-flow data processing, this smoothed MUSIC estimator seems to be more useful than the original one described in [11] because multiple slow-time ensembles with similar characteristics are generally not available for the estimation of the correlation matrix of each sample volume. Its efficacy in color-flow signal processing will be examined in our simulations as a comparison for the matrix pencil method.

### E. Computational Considerations

The matrix pencil estimator can be expected to have a higher computational burden than the lag-one autocorrelator that is widely used in color-flow data processing. In particular, the matrix pencil involves the use of SVD to carry out rank reduction on the matrix pair $[\mathbf{A}_1, \mathbf{A}_0]$, and it also requires the use of an eigenvalue solver to compute the principal frequency estimates. As shown elsewhere (see Table 3-2 in [18]), the matrix pencil needs on the order of $P^3$ floating point operations (flops) for each estimation

run. Therefore, this estimator is slightly more efficient than the MUSIC estimator that generally requires on the order of $N_D^3$ flops [12], but it is two orders of magnitude more complex than the lag-one autocorrelator that only requires on the order of $N_D$ flops (by inspection of the formulation in [1]). To improve the computational efficiency of the matrix pencil, it is possible to use more efficient SVD algorithms and eigenvalue solvers that exploit the Hankel matrices inherent in this estimator [19].

### III. APPLICATIONS OF MATRIX PENCIL IN COLOR-FLOW DATA PROCESSING

### A. Rank-One Matrix Pencil

As outlined in Table I, the matrix pencil estimator has several potential applications in color-flow data processing. For example, by assuming a rank-one signal eigen-structure (i.e., setting $K = 1$), this parametric estimator can be used to compute the mode frequency of any filtered slow-time signal. Note that the rank-one matrix pencil estimator can be considered as a generalized form of the lag-one autocorrelator [1]. Specifically, the rank-one estimator is a more advanced autocorrelator that has rank reduction capabilities depending on the choice of the pencil dimension $P$. As such, when the pencil dimension is greater than one ($P > 1$), the rank-one matrix pencil is less prone to noise perturbations than the original lag-one autocorrelator. On the other hand, when the pencil dimension is set equal to one (i.e., when $P = 1$), the two estimators become equivalent in their form as shown in Appendix B.

### B. Rank-Two Matrix Pencil

Besides computing modal frequencies from filtered slow-time data, the matrix pencil can also be used to obtain flow estimates in the presence of clutter. In particular, by assuming a higher-rank signal eigen-structure, the matrix pencil can be applied directly to the raw slow-time data to extract the modal Doppler frequency of blood echoes. One type of higher-rank matrix pencil estimator that is

useful in color-flow data processing is the rank-two approach that models the raw slow-time signal as a sum of two principal complex sinusoids (i.e., it assumes $K = 2$). The rank-two matrix pencil, which is similar to second-order AR modeling and rank-two MUSIC, assumes that one of the principal complex sinusoids corresponds to clutter and the other corresponds to blood echoes. In turn, it obtains the modal frequency of blood echoes from the larger (magnitude-wise) of the two principal frequencies. In terms of its use in flow studies, this rank-two estimator is suitable for finding the modal frequency of blood echoes in studies where the clutter is narrowband in nature with respect to the Doppler spectral resolution. Note that, as shown in Appendix B, the rank-two matrix pencil essentially degenerates to a second-order AR estimator when the pencil dimension is set equal to two (i.e., when $P = 2$).

### C. Rank-Adaptive Matrix Pencil

The rank-two matrix pencil estimator inherently assumes that clutter in the raw slow-time signal can be adequately modeled as a single complex sinusoid. However, such assumption may not always be valid because tissue motion can give rise to clutter with wideband characteristics. Consequently, the rank-two matrix pencil may sometimes give modal flow estimates that are inconsistent with the actual flow dynamics. This problem is generally more significant for slow-time data acquired using higher frequencies or longer ensemble periods because the Doppler spectral resolution is finer in these cases.

To address the theoretical limitation of the rank-two matrix pencil, it is worthwhile to consider the development of an algorithm for the matrix pencil to select its eigen-structure rank adaptively based on the Doppler spectral characteristics. One way of designing such algorithm is to analyze the spectral spread of the matrix pencil frequency estimates obtained for different eigen-structure ranks. In particular, it can be expected that, for cases with dominating wideband clutter, the spectral spread of lower-rank matrix pencil estimates should be smaller because the most dominant frequencies would likely correspond to clutter. Hence, as illustrated in the flowchart in Fig. 3, the rank selection algorithm can involve a search for the minimum eigen-structure rank that yields matrix pencil estimates with spectral spread greater than a certain threshold $\Delta f_{\text{thr}}$. The nominal rank $K_{\text{nom}}$ obtained from this algorithm can be expressed as:

$$K_{\text{nom}} = \arg\min_K \Big( \max\{f_{\text{D},1}, f_{\text{D},2}, \ldots, f_{\text{D},K}\}$$
$$- \min\{f_{\text{D},1}, f_{\text{D},2}, \ldots, f_{\text{D},K}\} > \Delta f_{\text{thr}} \Big). \quad (6)$$

The efficacy of this rank selection algorithm primarily depends on the choice of the spectral spread threshold $\Delta f_{\text{thr}}$, which is a quantity analogous to the stopband of a clutter filter. Once the rank has been adaptively estimated, the modal frequency of blood echoes can then be set equal to
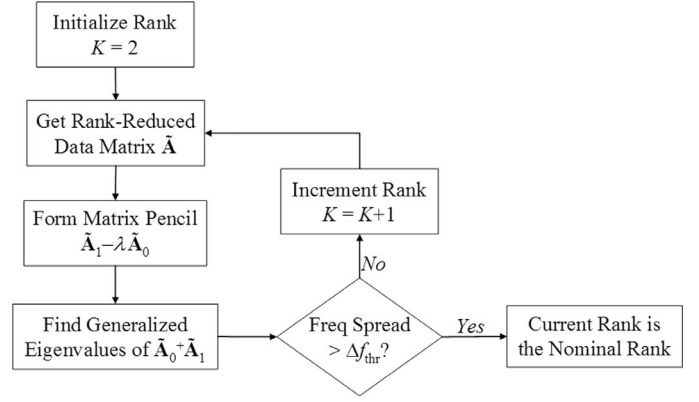


Fig. 3. Flowchart of the rank selection algorithm used for rank-adaptive matrix pencil. The algorithm is based on analyzing the spectral spread of matrix pencil frequency estimates obtained for each eigen-structure rank.
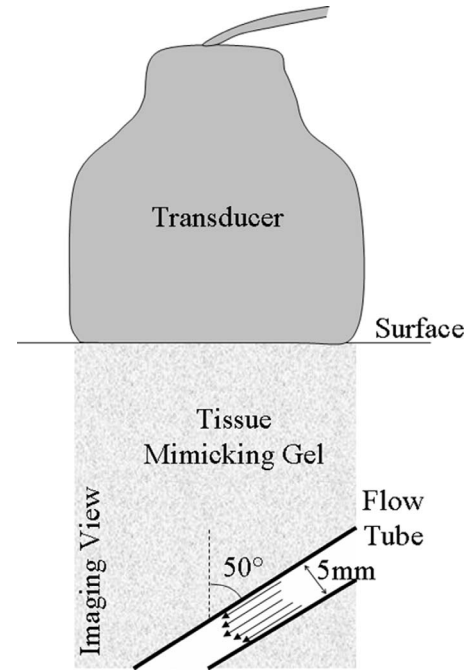


Fig. 4. Illustrating the physical setup used in the in vitro flow phantom study.

the frequency with largest magnitude in the set of $K_{\text{nom}}$ matrix pencil estimates.

## IV. In Vitro Imaging Experiment

As a preliminary assessment of the matrix pencil estimators, an in vitro imaging study was performed using a commercial flow phantom with known flow conditions. As shown in Fig. 4, the imaging view of this experiment is an in-plane slice of a Gammex-RMI phantom (Model 1425A, Middleton, WI) that has a 5 mm-diameter flow tube surrounded by rigid tissue-mimicking material and angled at 50° with respect to the surface. Note that the bottom-center of the imaging view was aligned with the flow phan-

TABLE II
PARAMETERS IN THE FLOW PHANTOM STUDY.

| Parameter | Value |
|---|---|
| Flow Phantom Parameters | |
| Acoustic speed | 1540 m/s |
| Beam-flow angle | 50° |
| Tube inner diameter | 5 mm |
| Flow profile | Steady, parabolic flow |
| Centerline flow velocity | 70 cm/s |
| Clutter-to-blood-signal ratio | In the range 20-30 dB |
| Data Acquisition Parameters | |
| Transmit pulse frequency | 5 MHz |
| Transmit pulse duration | 1.2 $\mu$s (6 cycles) |
| Pulse repetition interval | 0.175 ms |
| Slow-time ensemble size | 14 |
| Number of data frames | 5 |
| Image Size Parameters | |
| Lateral field of view | −19.2 to +19.2 mm |
| Number of beam lines | 257 |
| Axial field of view | +24.5 to +50.0 mm |
| Number of depth samples (per beam) | 166 (non-overlapping) |

tom's distal tube wall during the data acquisition. Also, the flow settings on the user interface of the Gammex-RMI system were adjusted to generate a steady flow profile with a centerline velocity of 70 cm/s. Given this setup, five frames of raw color-flow data were acquired for offline processing using an experimental scanner (ZONARE Medical Systems, Mountain View, CA) that can simultaneously acquire data over multiple beam lines via a zone-based data acquisition strategy [20]. A summary of the data acquisition parameters used in this in vitro study is provided in Table II.

### A. Signal Processing Procedure

As a preprocessing step, the slow-time ensembles of each data frame were first derived from the RF data stored internally in the scanner's channel domain memory [20]. Subsequently, the rank-one and rank-two matrix pencil estimators were applied to each slow-time ensemble to obtain flow estimates for all the sample volumes within the imaging view. It should be pointed out that the rank-adaptive matrix pencil estimator was not considered in this study because the slow-time clutter produced by the flow phantom was known to be relatively narrowband. Instead, the lag-one autocorrelator [1] was considered and used for comparison with the rank-one and rank-two matrix pencil estimators. Note that, for the autocorrelator and the rank-one matrix pencil estimator, a fifth-order projection-initialized IIR filter was used to suppress slow-time clutter prior to flow estimation (other types of filters may be used instead to obtain similar performance insights for these two estimators). Also, for both matrix pencil estimators, the pencil dimension parameter $P$ was set to $N_D/2$ (i.e., the maximum possible value).

Prior to display, the computed flow estimates over the imaging view were passed through a $5 \times 5$ median filter and a $5 \times 5$ mean filter to reduce the estimation variance. The smoothed velocity estimates were then converted into color pixels based on the unaliased velocity range and were superimposed onto a B-mode image for duplex display. Note that, in displaying the velocity maps, we made use of the filtered signal power as the color display gain criterion (i.e., velocity pixel is displayed only if the filtered signal power is above a threshold). For the rank-two matrix pencil estimator, which does not involve clutter filtering, this power quantity was estimated from the squared sum of singular values for SVD component orders greater than and equal to two. Such an estimation approach is fundamentally based on (7) in [10], where in this case the clutter eigen-space dimension was assumed to be one (since clutter was modeled as a single complex sinusoid by the rank-two matrix pencil).

### B. Data Analysis Protocol

As an analysis benchmark, a simulated color-flow map of the imaging view was first generated based on the fact that a parabolic flow profile with a centerline velocity of 70 cm/s was used in this in vitro study. This flow map, which is shown in Fig. 5(a), was then used to evaluate the ability of both matrix pencil flow estimators to reconstruct the flow dynamics of the phantom. To facilitate quantitative evaluation, we computed the correlation coefficient between the theoretical flow profile and each flow velocity map obtained from the estimators. Such performance measures can be expected to be close to unity if the reconstructed flow maps were similar to the simulated flow map.

### C. Color Flow Image Results

Figs. 5(b) through (d), respectively, show the velocity maps obtained from the lag-one autocorrelator, the rank-one matrix pencil, and the rank-two matrix pencil for a representative frame in the in vitro dataset. These images indicate that all three estimators seem capable of reconstructing velocity maps that are in reasonable qualitative agreement with the simulated theoretical flow profile (at least they have indicated a presence of flow only within the same spatial region depicted in the theoretical profile). Nevertheless, as suggested by its higher correlation coefficient, the rank-two matrix pencil estimator appears to show a better resemblance of the phantom's parabolic flow gradient. On the other hand, among the two estimators that involve clutter filtering, the rank-one matrix pencil estimator seems to give a somewhat more consistent flow map than that provided by the lag-one autocorrelator (whose correlation coefficient is 0.015 lower). Although these results are of qualitative nature, they do suggest that the matrix pencil method has potential in obtaining flow estimates that are less prone to the biasing effect of the clutter filter.

(a) Simulated Profile

(b) Lag-One Autocorrelator
Corr. Coeff. = 0.9489 ± 0.0025

(c) Rank-One Matrix Pencil
Corr. Coeff. = 0.9640 ± 0.0032

(d) Rank-Two Matrix Pencil
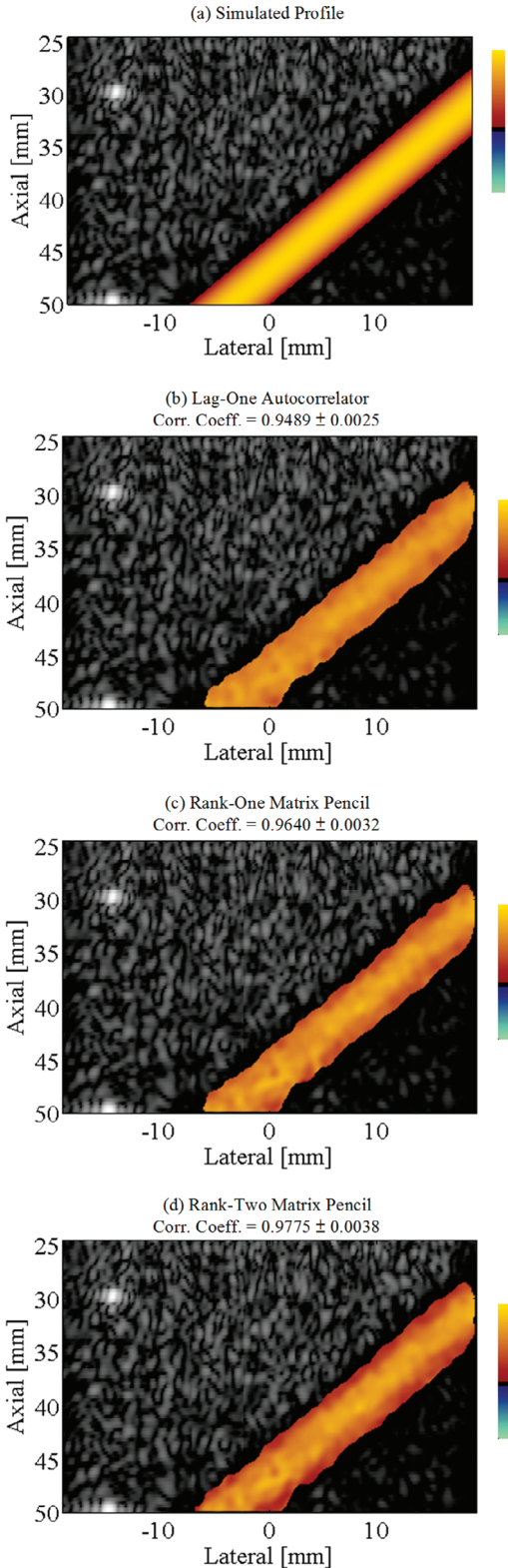Corr. Coeff. = 0.9775 ± 0.0038

Fig. 5. The simulated flow profile of the phantom [as seen in (a)] and the corresponding velocity maps [(b), (c), and (d)] obtained for one of the five frames in the color flow dataset. The correlation coefficients of the velocity maps are also provided. These velocity maps were obtained using the processing parameters described in Section IV-A. Their unaliased velocity range was between −61.6 cm/s and +75.3 cm/s, and they had the same color display gain.

TABLE III
SIMULATION PARAMETERS.

| Parameter | Value |
|---|---|
| **Fixed Parameters** | |
| Acoustic speed, $c_o$ | 1540 m/s |
| F-number, $F_{\mathrm{num}}$ | 4 |
| Pulse carrier frequency, $f_o$ | 5 MHz |
| Pulse repetition interval, $T_{\mathrm{PRI}}$ | 1.0 ms |
| Beam-flow angle, $\theta_b$ | 60° |
| Beam-tissue angle, $\theta_c$ | 0° |
| Slow-time ensemble size, $N_D$ | 10 |
| Dynamic range | 14 bits |
| Number of realizations per dataset | 10000 |
| Clutter-to-blood signal ratio, CBR | 30 dB |
| Average noise strength, $\kappa_w$ | 10 dB |
| Tissue vibration frequency, $f_{\mathrm{vib}}$ | 5 Hz |
| **Variable Parameters** | |
| Blood velocity, $v_b$ | 0 to $v_{\mathrm{alias}}$ |
| Blood-signal-to-noise ratio, BSNR | −20 to +30 dB |
| Maximum tissue velocity, $v_{c,\mathrm{max}}$ | 0 or 1 cm/s |
| **Responding Parameters** | |
| Aliasing velocity, $v_{\mathrm{alias}}$ | 15.4 cm/s |
| Ensemble period, $N_D T_{\mathrm{PRI}}$ | 10.0 ms |
| Max. instantaneous clutter phase, $\phi_{c,\mathrm{max}}$ | 0 or 13.0 radians |
| Maximum clutter frequency | 0 or 70 Hz |

## V. SIMULATION METHODS

To further investigate the performance of the matrix pencil method, we carried out a series of simulation studies using the synthesis model described in Section III of [10]. In particular, two rounds of simulations were conducted to analyze the efficacy of the matrix pencil quantitatively under various flow scenarios and noise levels. The first round of simulations, which involved the modeling of a flow scenario with no tissue motion, aimed to evaluate the performance of rank-one and rank-two matrix pencil estimators at different pencil dimensions, BSNRs, and flow velocities. With the insights gained from the initial simulations, a second round of simulations based on a flow scenario with moving tissue was then performed to study the efficacy of a rank-adaptive matrix pencil and the spectral spread criterion proposed for rank selection.

### A. Simulation Parameters

The data synthesis parameters used in the simulations are listed in Table III. For this study, slow-time datasets (each with 10 000 realizations) were synthesized for blood velocities $(v_b)$ ranging from zero to the aliasing limit (15.4 cm/s) as well as BSNRs ranging from −20 to 30 dB to assess the performance of the matrix pencil estimator. Note that, to simulate scenarios with and without tissue motion, the maximum tissue velocity $(v_{c,\mathrm{max}})$ was set to either 0 or 1 cm/s. In terms of the major fixed parameters, the ultrasound frequency $(f_o)$ and the pulse repetition interval $(T_{\mathrm{PRI}})$ were, respectively, set to 5 MHz and 1.0 ms to model data acquisition in a typical low-velocity vascular imaging scenario. As well, the average strength of slow-

time clutter was defined to be 30 dB greater than that of blood, and a slow-time ensemble size of ten samples was used for the synthesized datasets.

### B. Analysis Protocol

Flow estimation was performed using four different frequency-based methods: lag-one autocorrelator [1], the matrix pencil, AR modeling (using a forward-backward fitting approach) [6], and data-smoothed Root-MUSIC [16]. The estimation process was carried out on all the synthesized slow-time datasets to assess the performance of each method. For the autocorrelator and the rank-one matrix pencil estimator, the same filter type as used in the flow phantom study (i.e., fifth-order IIR filter, projection-initialized) was applied to suppress clutter prior to flow estimation. As for the rank-adaptive matrix pencil estimator, a two-way spectral spread threshold of 150 Hz was used for the rank selection algorithm. It should also be pointed out that, to avoid aliasing problems during the analysis, all flow estimates were partially unwrapped in velocity so that they are bounded within the range $v_b \pm v_{\text{alias}}$, where $v_{\text{alias}}$ is the aliasing velocity. This partial unwrapping procedure ensures that, if an estimator is unbiased, the distribution of velocity estimates is centered about $v_b$ with no discontinuity.

In our analysis, two performance measures were used to assess an estimator's performance quantitatively: 1) the mean estimation bias, and 2) the root-mean-squared (RMS) estimation error. The mean estimation bias was computed by finding the average difference between the estimated velocity and the actual blood velocity used to synthesize the slow-time signal. It is well established from estimation theory that a low bias is an indication of high estimation accuracy. On the other hand, the RMS estimation error was calculated by taking the square root of the average squared difference between the estimated velocity and the true blood velocity. For an estimator to have high accuracy and precision, its RMS estimation error should be low in general.

## VI. Simulation Results

### A. Flow Scenario with Clutter from Motionless Tissue

*1. Efficacy of Rank Reduction:* Fig. 6 shows the bias and the RMS error of this estimator for different pencil dimensions as a function of BSNR. Results are provided for both the rank-one and rank-two matrix pencil when the slow-time ensemble size is 10 samples, and they were obtained by processing slow-time data synthesized with a 5 cm/s blood velocity and clutter generated by motionless tissue. It can be seen that the estimation bias of both the rank-one and rank-two matrix pencil drops significantly at medium and low BSNRs with increasing pencil dimension. In addition, the RMS error either remains similar or decreases gradually when the pencil dimension becomes larger. These observations suggest that rank reduction can improve the matrix pencil method's

estimation performance. They also indicate that the flow-estimation performance is generally better at larger pencil dimensions: a result that can be expected because larger pencil dimensions give rise to more entries in the Hankel data matrix and in turn the rank reduction performance should be improved. Based on these grounds, it appears that the dimension parameter for the matrix pencil estimator should be set to the maximum possible value (i.e., $N_D/2$).

*2. Comparative Assessment at Different BSNRs:* In Fig. 7, the estimation performance of matrix pencil at various BSNRs is compared against the lag-one autocorrelator, the second-order AR estimator, and the rank-two Root-MUSIC estimator (with data smoothing). The shown results are based on slow-time data synthesized with blood velocities of 5 and 10 cm/s (i.e., mean blood Doppler frequencies of 162 and 325 Hz). In other words, these results correspond, respectively, to cases where the blood frequency contents are near and away from the stopband of the clutter filter. Note that, when using the matrix pencil estimator to process the synthesized slow-time data, the pencil dimension was defined as $N_D/2$ to maximize the rank reduction performance. Likewise, when using the data-smoothed MUSIC estimator, a window size of $N_D/2$ was chosen to form the slow-time correlation matrix.

From Fig. 7, it can be seen that the rank-one matrix pencil (black dashed line) is less biased than the autocorrelator (gray dashed line) for all BSNRs. The rank-one matrix pencil also appears to be more precise than the autocorrelator when the blood frequency contents are close to filter stopband (as seen for the case where the blood velocity is 5 cm/s). Both of these findings are consistent with our previous observations on the efficacy of rank reduction in the matrix pencil estimator. Another observation worth noting is that, for the 5 cm/s blood velocity case, distortions from the clutter filter cause both the rank-one matrix pencil and the lag-one autocorrelator to remain biased even at high BSNRs. On the other hand, all three rank-two flow estimators that do not involve clutter filtering are not prone to these distortions. In comparison between the rank-two estimators, the rank-two matrix pencil (black solid line) is significantly more accurate than the second-order AR estimator (gray dotted line) at medium and low BSNRs, and it appears to share similar performance trends with the rank-two Root-MUSIC estimator (gray solid line). This result can be expected because the matrix pencil and Root-MUSIC both involve an orthogonal decomposition (either through SVD or eigen-decomposition) in their theoretical formulation to help separate signal components from noise (as noted in Section II-C).

*3. Comparative Assessment at Different Blood Velocities:* Fig. 8 shows the bias and the RMS error of various frequency-based flow estimators as a function of the blood velocity for BSNRs of 0 and 10 dB. As can be seen, the rank-one matrix pencil and the lag-one autocorrelator both exhibit substantial estimation bias at low blood ve-
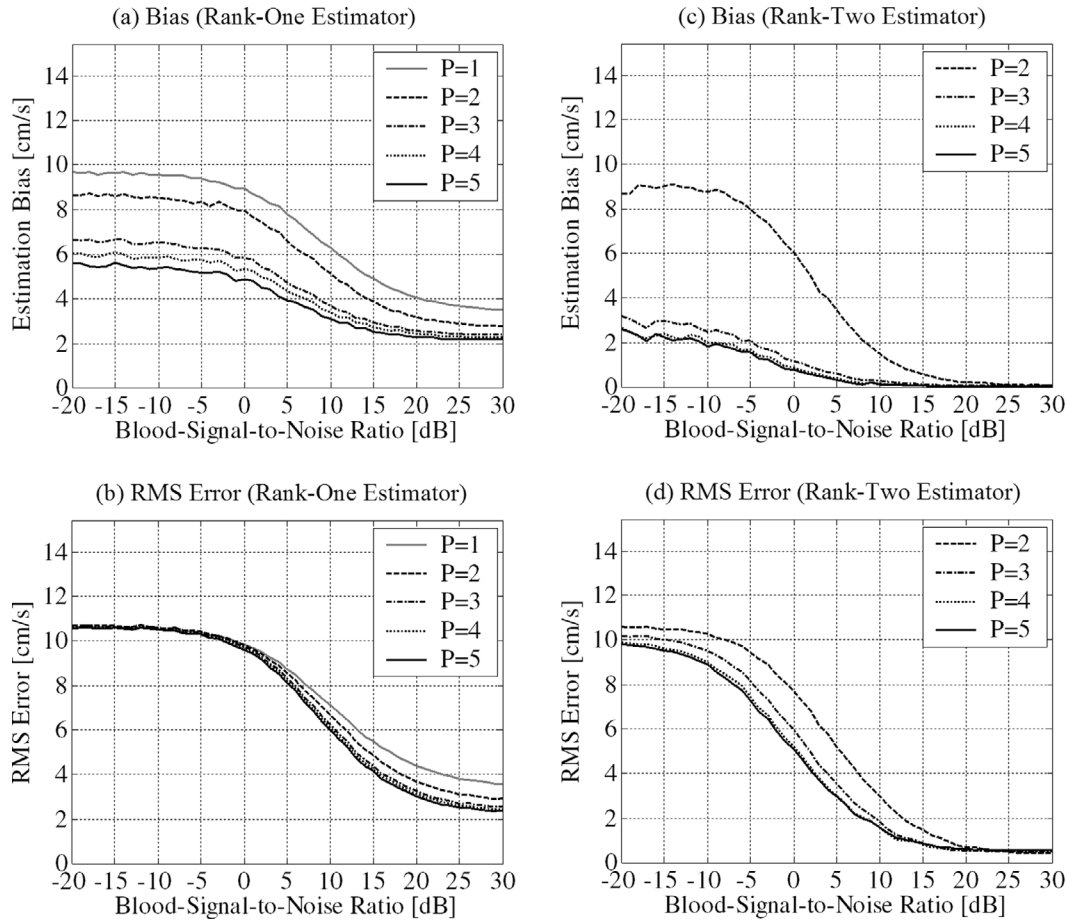
Fig. 6. Estimation performance of rank-one and rank-two matrix pencil estimators in the flow scenario with clutter from motionless tissue. In (a) and (b), the estimation biases and the RMS errors are shown for the rank-one estimator at various BSNRs and pencil dimensions. The corresponding results for the rank-two estimator are shown in (c) and (d). Note that the true blood velocity used to synthesize the slow-time data is 5 cm/s.

locities because of clutter filter distortions on the blood signal (in the form of partial or complete attenuation). In fact, their bias is at a maximum for blood velocities near 4 to 5 cm/s, corresponding to blood Doppler frequencies in the range of 130 to 160 Hz. Note that the blood spectral components at these velocities are mainly located inside the clutter filter's transition region. On the other hand, the rank-two matrix pencil and rank-two Root-MUSIC both have significantly lower biases than the other estimators at any blood velocity. This observation is in agreement with our results presented for different BSNR levels. It is also worth pointing out that, at higher blood velocities, the precision of the rank-one matrix pencil and the autocorrelator appears to be slightly better. This phenomenon can be explained by recognizing that, for these two estimators, the clutter filtering step prior to flow estimation has more or less suppressed some of the background white noise and hence the estimation variance is inherently lower.

### B. Flow Scenario with Clutter from Moving Tissue

*1. Efficacy of Adaptive Rank Selection:* To demonstrate the need for adaptive rank selection when using the matrix pencil, we first studied the estimation performance of

a rank-two matrix pencil in the flow scenario with clutter generated by moving tissue. In this study, the flow estimates of a rank-two matrix pencil were evaluated for cases with blood velocities of 5 and 10 cm/s as well as a BSNR of 10 dB. The upper half of Fig. 9 shows the corresponding distribution for 10 000 estimates of the blood Doppler frequency (prior to velocity conversion) in the two cases. As can be seen, a number of rank-two matrix pencil estimates are biased toward zero: a result that is inconsistent with the flow dynamics because blood velocities of 5 and 10 cm/s, respectively, give rise to mean blood Doppler frequencies of 162 and 325 Hz. In fact, when the blood velocity is 5 cm/s, it was found that 19.2% of the flow estimates in this dataset have a magnitude lower than the approximate clutter range of ±70 Hz; likewise, when the blood velocity is 10 cm/s, 13.9% of the estimates were less than the peak clutter frequency. In contrast to the rank-two estimation results, the bottom half of Fig. 9 shows the distribution of blood Doppler frequencies found from a rank-adaptive matrix pencil estimator that uses a spectral spread threshold of 150 Hz during rank selection. Although favorable results were not observed (some overestimation was seen) for the case with 5 cm/s velocity, the histogram for the higher velocity case (10 cm/s) revealed
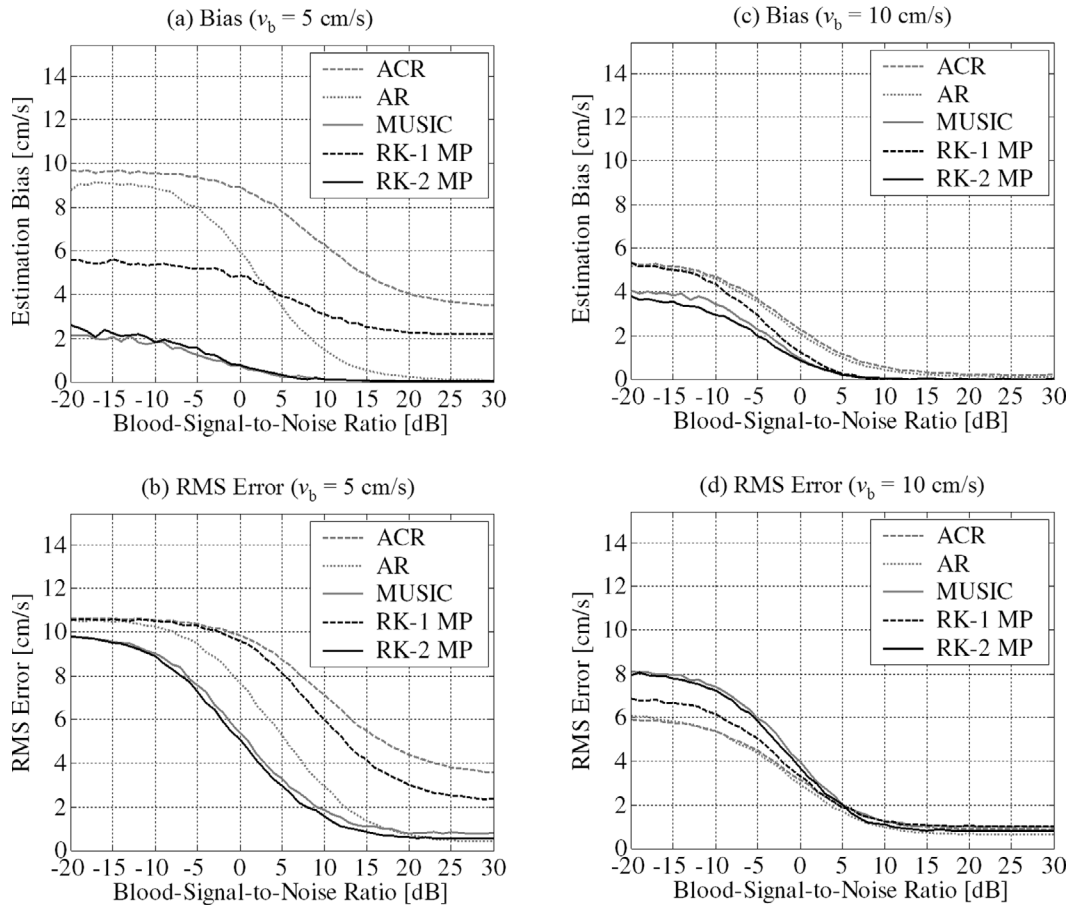
Fig. 7. Estimation performance of various frequency-based flow estimators in the flow scenario with clutter from motionless tissue. In (a) and (b), the estimation bias and the RMS error at various BSNRs are shown for the case where the actual blood velocity is 5 cm/s. The corresponding results for the 10 cm/s blood velocity case are shown in (c) and (d). Note that a pencil dimension of $P = N_D/2$ was used for the matrix pencil estimators.

that the rank-adaptive matrix pencil is able to obtain flow estimates that are relatively centered at the mean blood frequency of the synthesized slow-time data. As such, the rank-adaptive matrix pencil appears to have better estimation accuracy than the rank-two counterpart at high blood velocities.

*2. Comparative Assessment at Different Blood Velocities:* For various blood velocities and two BSNR values, Fig. 10 compares the bias and the RMS error of the rank-adaptive matrix pencil (solid line) against those of the autocorrelator (dash-dotted line) as well as the rank-one (dotted line) and rank-two matrix pencil estimators (dashed line). It can be seen that in the higher blood velocity range ($> 1/2 v_{alias}$), the rank-adaptive matrix pencil is the most accurate (i.e., lowest bias) among the four estimators. However, in the lower blood velocity range ($< 1/2 v_{alias}$), the rank-adaptive matrix pencil appears to suffer a significant drop in the estimation precision. Such result is to be expected because the rank selection algorithm used in this study assumes that the slow-time clutter spans a prescribed bandwidth and therefore exhibits performance characteristics similar to the stopband of a clutter filter. In fact, as can be seen from Fig. 10, the es-

timation precision of the rank-adaptive matrix pencil is quite similar to that for the autocorrelator and rank-one matrix pencil, both of which involves the use of a clutter filter. It is also worth pointing out that the better accuracy and precision seen for a rank-two matrix pencil at lower velocities is a somewhat misleading result since this estimator gives flow estimates that are always biased toward zero, and hence it tends to yield lower estimation errors when the actual blood velocity is low. Note that the use of a rank-two matrix pencil in flow scenarios with clutter arising from moving tissue can be considered as being analogous to applying a correlation-based estimator to color flow data whose clutter has not been adequately suppressed.

## VII. CONCLUSION

It has been the intent of this paper to investigate the use of the matrix pencil estimation framework in color-flow data processing under various BSNRs and flow conditions. In our theoretical formulation, we have first considered a type of fixed-rank matrix pencil estimator called rank-one matrix pencil and have shown that it is a generalized form
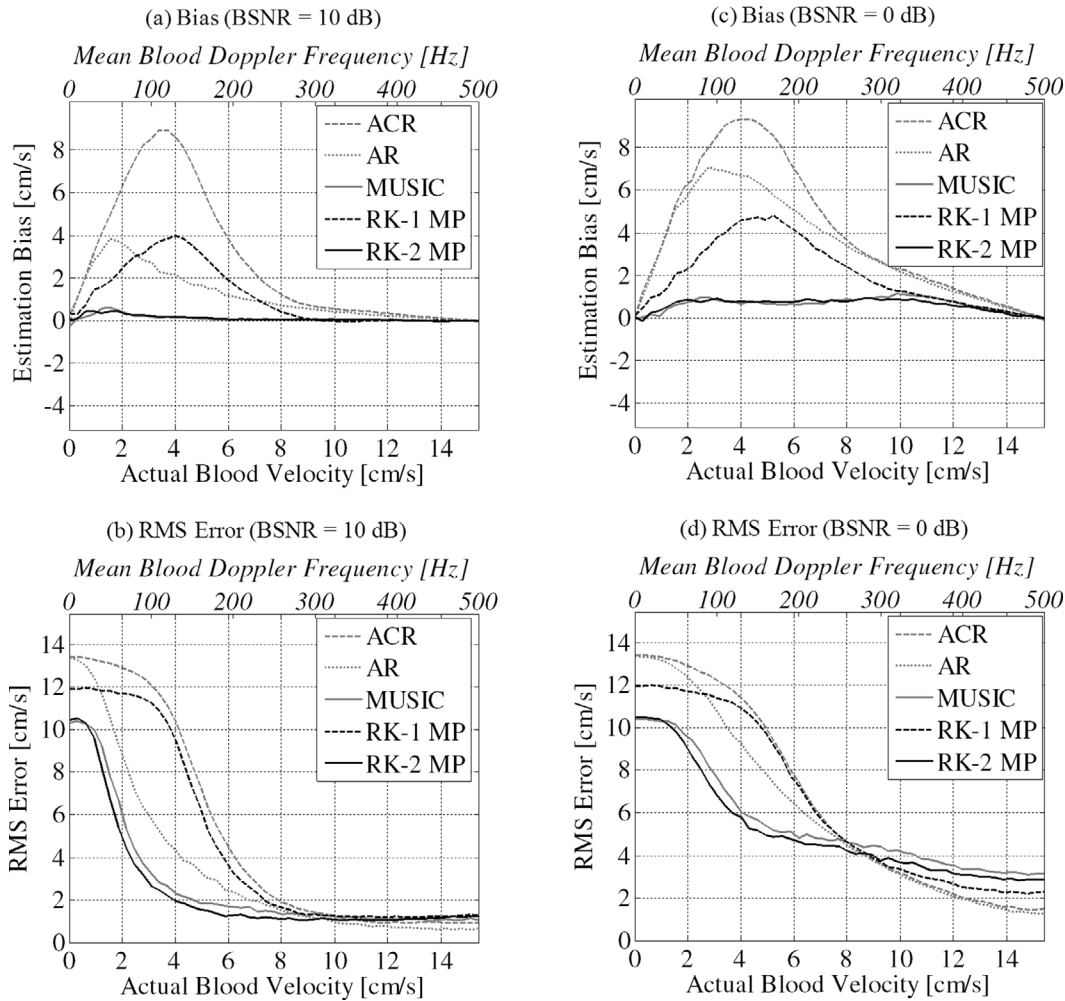
Fig. 8. Estimator performance as a function of blood velocity in the flow scenario with clutter from motionless tissue. In (a) and (b), the estimation bias and the RMS error are shown for the case where the BSNR is 10 dB. In (c) and (d), similar results are shown for a BSNR of 0 dB. For the matrix pencil estimators, a pencil dimension of $P = N_D/2$ was used.

of the lag-one autocorrelator that is often used in color-flow data processing. To realize the potential of the matrix pencil in obtaining flow estimates directly from the raw slow-time data, we have considered the use of a rank-two matrix pencil estimator and have shown that it is suitable for use in flow scenarios where the slow-time clutter can be sufficiently modeled as a single complex sinusoid. Besides fixed-rank matrix pencil estimators, we have also developed an adaptive-rank matrix pencil estimator that can be used to obtain flow estimates in the presence of wideband slow-time clutter. The rank selection algorithm used in rank-adaptive matrix pencil is based on a search of the minimum eigen-structure rank that yields a matrix pencil spectral spread greater than a certain bandwidth.

Our performance analysis has demonstrated that the rank-one matrix pencil is more accurate and precise than the lag-one autocorrelator at various BSNRs. Results have also shown that, in flow scenarios with narrowband slow-time clutter, the rank-two matrix pencil is even more accurate than the rank-one matrix pencil because the former does not suffer from potential biases due to clutter filtering. On the other hand, in flow scenarios with slow-time

clutter arising from moving tissue, the rank-adaptive matrix pencil has shown to be more useful because it can give velocity estimates that are more consistent with the actual flow dynamics, provided that the blood spectral components are outside the specified clutter bandwidth. These findings indicate that the matrix pencil framework is potentially useful in color-flow signal processing.

## APPENDIX A
## THEORETICAL DETAILS OF THE MATRIX PENCIL METHOD

### A. Relationship Between Generalized Eigenvalues and Principal Frequencies

To appreciate how the matrix pencil $\mathbf{A}_1 - \lambda\mathbf{A}_0$ gives GEs that correspond to the principal frequencies, it is necessary to consider the decomposition properties of the two data matrices. In particular, with reference to the signal model given in (1), the data matrices $\mathbf{A}_1$ and $\mathbf{A}_0$ in the absence of noise can be decomposed into the following forms [12]:
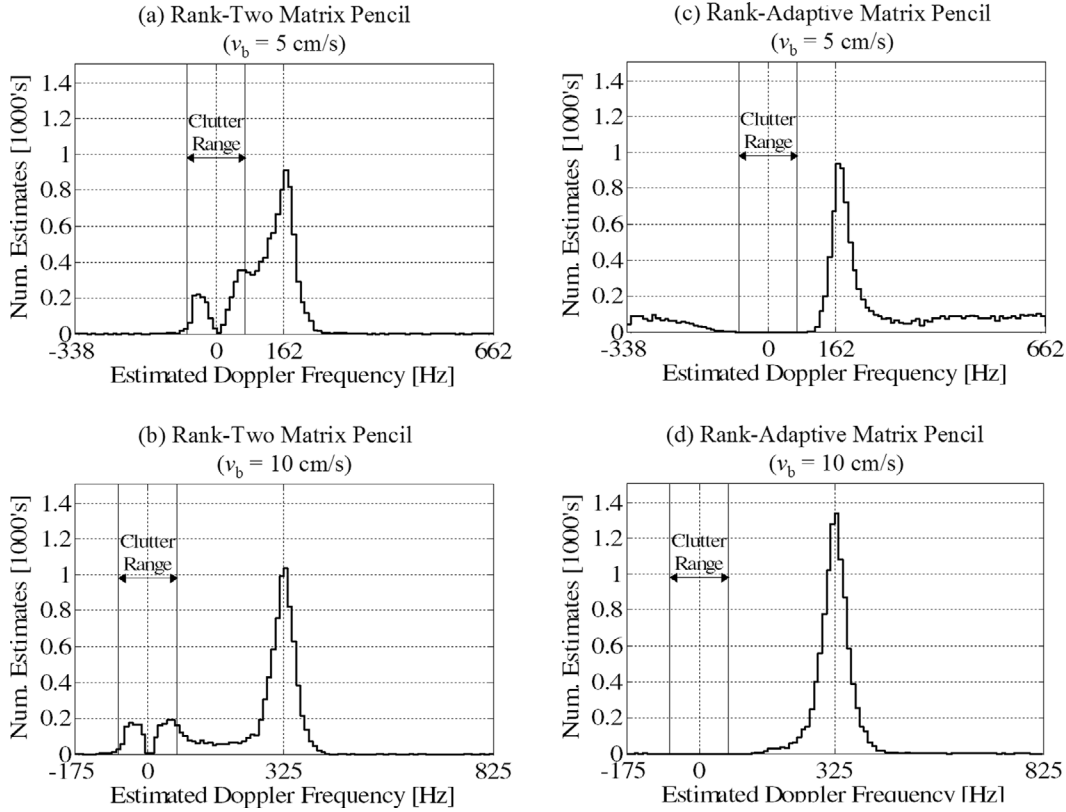
Fig. 9. Histograms of the blood frequency estimates obtained from the rank-two and rank-adaptive matrix pencil estimators for the flow scenario with clutter from moving tissue. Results for the rank-two estimator are shown in (a) and (b), while the ones for the rank-adaptive estimator are shown in (c) and (d). They correspond to cases where the blood velocity is 5 or 10 cm/s. Note that the flow estimates are displayed over the unaliased Doppler spectral range, and there are 10 000 estimates in each histogram.

$$\mathbf{A}_1 = \mathbf{Z}_L \mathbf{D} \boldsymbol{\Phi} \mathbf{Z}_R, \tag{A1}$$

$$\mathbf{A}_0 = \mathbf{Z}_L \mathbf{D} \mathbf{Z}_R, \tag{A2}$$

where the matrices $\mathbf{Z}_L$, $\mathbf{Z}_R$, $\mathbf{D}$, and $\boldsymbol{\Phi}$ are defined in (A3)–(A6) (see next page). Given these decomposed forms, the matrix pencil $\mathbf{A}_1 - \lambda \mathbf{A}_0$ can be expressed as:

$$\mathbf{A}_1 - \lambda \mathbf{A}_0 = \mathbf{Z}_L \mathbf{D} [\boldsymbol{\Phi} - \lambda \mathbf{I}] \mathbf{Z}_R. \tag{A7}$$

From the $\boldsymbol{\Phi} - \lambda \mathbf{I}$ term in the above expression, it can be seen that if $\lambda$ equals to any of the main diagonal entries in $\boldsymbol{\Phi}$ (i.e., any of $z_k$), then the rank of $\mathbf{A}_1 - \lambda \mathbf{A}_0$ is reduced by one. Hence, in the absence of noise, values of the set $\{z_k\}$ are indeed the GEs of $\mathbf{A}_1 - \lambda \mathbf{A}_0$. Note that, as reviewed by van der Veen *et al.* [13], the solution for $\boldsymbol{\Phi}$ in (A7) is equivalent to finding a rotational matrix operator such that the rotation is invariant from a subspace perspective (i.e., the two data matrices $\mathbf{A}_1$ and $\mathbf{A}_0$ span the same subspace). As such, the matrix pencil estimator can be considered as an estimation method that is based on rotational invariance principles.

### B. Mathematical Solution for Generalized Eigenvalues

To solve for the GEs of the matrix pair defined by (3) or (4), we can first rewrite the GE equation in (2) as a standard eigenvalue equation. This algebraic manipulation can be done by multiplying both sides of the GE equation with $\mathbf{A}_0^H$ and moving all matrix terms to one side of the equation. The resulting eigenvalue equation is then given by:

$$\left( \mathbf{A}_0^H \mathbf{A}_0 \right)^{-1} \mathbf{A}_0^H \mathbf{A}_1 \mathbf{q} = \lambda \mathbf{q} \iff \left[ \mathbf{A}_0^+ \mathbf{A}_1 - \lambda \mathbf{I} \right] \mathbf{q} = \mathbf{0}, \tag{A8}$$

where the '+' superscript refers to a pseudo-inverse operation (i.e., the singular matrix equivalent of a matrix inverse). From this expression, it can be seen that the GEs of $\mathbf{A}_1 - \lambda \mathbf{A}_0$ (or $\tilde{\mathbf{A}}_1 - \lambda \tilde{\mathbf{A}}_0$) are essentially the eigenvalues of $\mathbf{A}_0^+ \mathbf{A}_1$ (or $\tilde{\mathbf{A}}_0^+ \tilde{\mathbf{A}}_1$). Hence, it is possible to use a standard eigenvalue solving algorithm such as QR factorization or power iterations to compute the GEs [19].

### APPENDIX B
### RELATIONSHIP BETWEEN MATRIX PENCIL AND EXISTING ESTIMATORS

#### A. Rank-One Matrix Pencil

When $P = 1$, the rank-one matrix pencil estimator is equivalent to the lag-one autocorrelator. This equivalence can be shown by noting that, for a given filtered slow-time signal $y(n)$, the matrices $\mathbf{A}_1$ and $\mathbf{A}_0$ in the matrix pencil estimator degenerate to the following vectors (of size $N_D - 1$) in the limiting case:
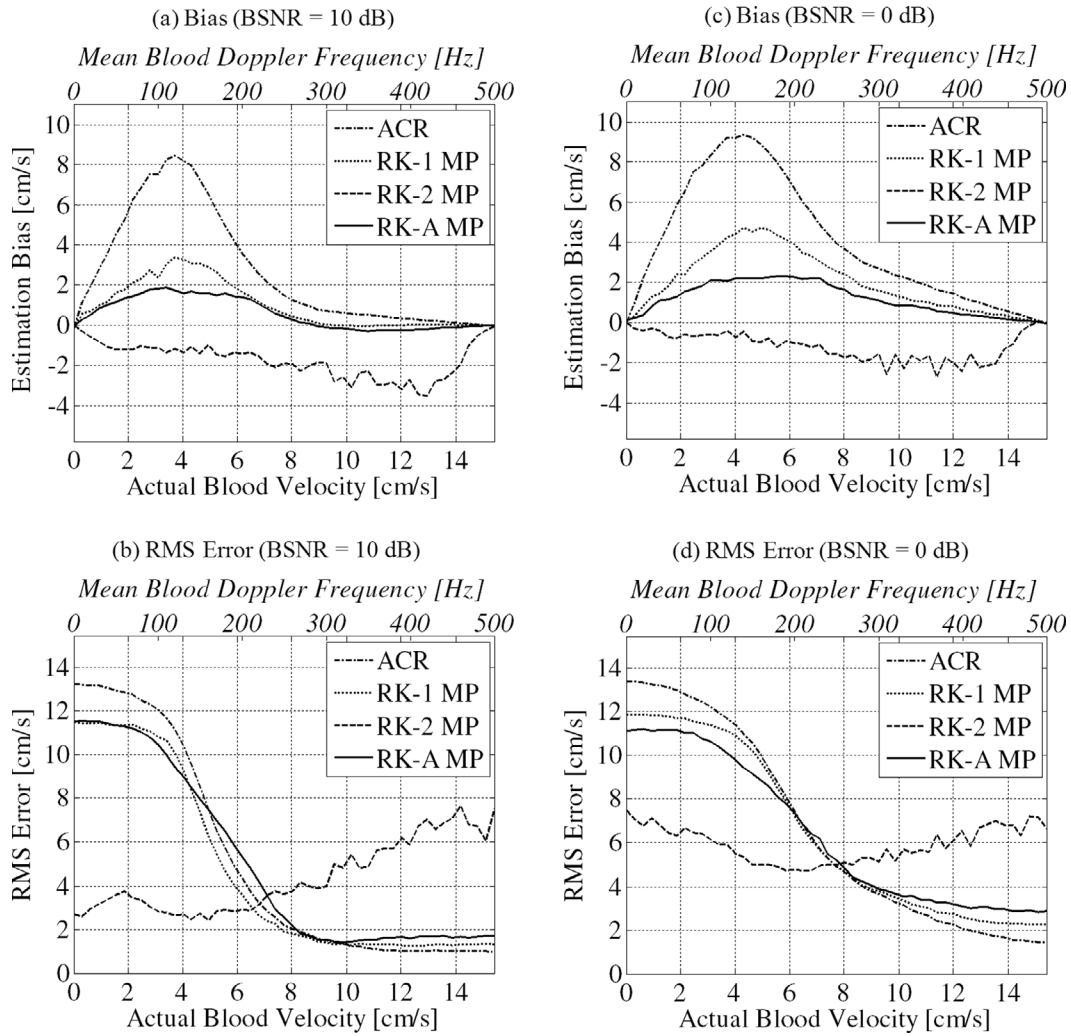
Fig. 10. Estimation performance of flow estimators in the flow scenario with clutter from moving tissue. In (a) and (b), the estimation bias and the RMS error as a function of blood velocity are shown for the case where the BSNR is 10 dB. Similar results for a BSNR of 0 dB are shown in (c) and (d). A pencil dimension of $P = N_D/2$ was used for matrix pencil.

$$\mathbf{Z}_{\mathrm{L}} =$$

$$\begin{bmatrix} 1 & 1 & \cdots & 1 \\ z_1 & z_2 & \cdots & z_K \\ \vdots & \vdots & \ddots & \vdots \\ z_1^{(N_D-P-1)} & z_2^{(N_D-P-1)} & \cdots & z_K^{(N_D-P-1)} \end{bmatrix}_{(N_D-P) \times K} \Bigg|_{z_k = e^{j2\pi f_{\mathrm{D},k} T_{\mathrm{PRI}}}}, \tag{A3}$$

$$\mathbf{Z}_{\mathrm{R}} = \begin{bmatrix} 1 & z_1 & \cdots & z_1^{(P-1)} \\ 1 & z_2 & \cdots & z_2^{(P-1)} \\ \vdots & \vdots & \ddots & \vdots \\ 1 & z_K & \cdots & z_K^{(P-1)} \end{bmatrix}_{K \times P} \Bigg|_{z_k = e^{j2\pi f_{\mathrm{D},k} T_{\mathrm{PRI}}}}, \tag{A4}$$

$$\mathbf{D} = diag\{\chi_1, \chi_2, \ldots, \chi_K\}, \tag{A5}$$

$$\mathbf{\Phi} = diag\{z_1, z_2, \ldots, z_K\}\big|_{z_k = e^{j2\pi f_{\mathrm{D},k} T_{\mathrm{PRI}}}}. \tag{A6}$$

$$\mathbf{a}_1 = [y(1), y(2), \ldots, y(N_D - 1)], \tag{B1}$$

$$\mathbf{a}_0 = [y(0), y(1), \ldots, y(N_D - 2)]. \tag{B2}$$

From the expressions given in (5), $\mathbf{a}_1$ and $\mathbf{a}_0$ would form a matrix pencil that gives the following modal frequency estimate:

$$f_{\mathrm{D(est)}} = \frac{1}{2\pi T_{\mathrm{PRI}}} \arg\{\lambda\} \text{ for } \lambda = \frac{\mathbf{a}_0^{\mathrm{H}} \mathbf{a}_1}{\mathbf{a}_0^{\mathrm{H}} \mathbf{a}_0} = \frac{R_y(1)}{R_y(0)}, \tag{B3}$$

where $R_y(0)$ and $R_y(1)$ are, respectively, the lag-zero and lag-one autocorrelation functions of the filtered slow-time signal. Since $R_y(0)$ is always a real quantity (it is simply the squared-norm of $\mathbf{a}_0$), (B3) is essentially equivalent to the formulation presented in [1], thereby confirming the equivalence between the rank-one matrix pencil and the lag-one autocorrelator when the pencil dimension is equal to one.

### B. Rank-Two Matrix Pencil

When $P = 2$, the rank-two matrix pencil estimator is equivalent to a second-order AR estimator. To show this equivalence, we can first note that the matrix pair $[\mathbf{A}_1, \mathbf{A}_0]$ for the matrix pencil and the solution matrix $\mathbf{A}_0^+ \mathbf{A}_1$ would take on the following forms when $P = 2$ [12]:

$$\mathbf{A}_1 = \begin{bmatrix} x(1) & x(2) \\ \vdots & \vdots \\ x(N_D - 2) & x(N_D - 1) \end{bmatrix}, \tag{B4}$$

$$\mathbf{A}_0 = \begin{bmatrix} x(0) & x(1) \\ \vdots & \vdots \\ x(N_D - 3) & x(N_D - 2) \end{bmatrix}, \tag{B5}$$

$$\mathbf{A}_0^+ \mathbf{A}_1 = \begin{bmatrix} 0 & c_1 \\ 1 & c_2 \end{bmatrix}, \tag{B6}$$

where $c_1$ and $c_2$ are, respectively, the product coefficients between $\mathbf{A}_0^+$ and the last column of $\mathbf{A}_1$. Note that the matrix shown in (B6) is the same as the companion matrix of a second-order AR polynomial, and its two eigenvalues are indeed the roots of the AR polynomial. Therefore, when $P = 2$, the rank-two matrix pencil and the second-order AR estimator are equivalent in formulation. On the other hand, by using a larger pencil dimension (i.e., setting $P > 2$), the rank-two matrix pencil can be made less sensitive to noise perturbations through matrix rank reduction (just like the rank-one formulation). It is worth mentioning that, to achieve the same advantage with AR modeling, an SVD truncation step may be included in the least-squares fit between the regressive signal model and the raw slow-time data [21]. Nevertheless, Hua and Sarkar [15] have shown that the SVD-based AR modeling method is not as effective as the matrix pencil.

## References

[1] C. Kasai, K. Namekawa, A. Koyano, and R. Omoto, "Real-time two-dimensional blood flow imaging using an autocorrelation technique," *IEEE Trans. Sonics Ultrason.*, vol. 32, pp. 458–464, 1985.

[2] T. Loupas, J. T. Powers, and R. W. Gill, "An axial velocity estimator for ultrasound blood flow imaging, based on a full evaluation of the Doppler equation by means of a two-dimensional autocorrelation approach," *IEEE Trans. Ultrason., Ferroelect., Freq. Contr.*, vol. 42, pp. 672–688, 1995.

[3] O. Bonnefous and P. Pesque, "Time domain formulation of pulsed-Doppler ultrasound and blood velocity estimation by cross correlation," *Ultrason. Imag.*, vol. 8, pp. 73–85, 1986.

[4] K. W. Ferrara and V. R. Algazi, "A new wideband spread target maximum likelihood estimator for blood velocity estimation—Part I: Theory," *IEEE Trans. Ultrason., Ferroelect., Freq. Contr.*, vol. 38, pp. 1–16, 1991.

[5] S. K. Alam and K. J. Parker, "The butterfly search technique for estimation of blood velocity," *Ultrasound Med. Biol.*, vol. 21, pp. 657–670, 1995.

[6] Y. B. Ahn and S. B. Park, "Estimation of mean frequency and variance of ultrasonic Doppler signal by using second-order autoregressive model," *IEEE Trans. Ultrason., Ferroelect., Freq. Contr.*, vol. 38, pp. 172–182, 1991.

[7] P. J. Vaitkus and R. S. C. Cobbold, "A comparative study and assessment of Doppler ultrasound spectral estimation techniques. Part I: Estimation methods," *Ultrasound Med. Biol.*, vol. 14, pp. 661–672, 1988.

[8] A. C. H. Yu, K. W. Johnston, and R. S. C. Cobbold, "Frequency-based signal processing for ultrasound color flow imaging," *Can. Acoust.*, vol. 35, no. 2, pp. 11–23, 2007.

[9] M. E. Allam and J. F. Greenleaf, "Isomorphism between pulsed-wave Doppler ultrasound and direction-of-arrival estimation—Part I: Basic principles," *IEEE Trans. Ultrason., Ferroelect., Freq. Contr.*, vol. 43, pp. 911–922, 1996.

[10] A. C. H. Yu and R. S. C. Cobbold, "Single-ensemble-based eigen-processing methods for color flow imaging—Part I. The Hankel-SVD Filter," *IEEE Trans. Ultrason., Ferroelect., Freq. Contr.*, vol. 55, no. 3, pp. 559–572, 2008.

[11] P. J. Vaitkus and R. S. C. Cobbold, "A new time-domain narrowband velocity estimation technique for Doppler ultrasound flow imaging. Part I: Theory," *IEEE Trans. Ultrason., Ferroelect., Freq. Contr.*, vol. 45, pp. 939–954, 1998.

[12] P. J. Vaitkus, R. S. C. Cobbold, and K. W. Johnston, "A new time-domain narrowband velocity estimation technique for Doppler ultrasound flow imaging Part II: Comparative performance assessment," *IEEE Trans. Ultrason., Ferroelect., Freq. Contr.*, vol. 45, pp. 955–971, 1998.

[13] Y. Hua and T. K. Sarkar, "Matrix pencil method for estimating parameters of exponentially damped/undamped sinusoids in noise," *IEEE Trans. Acoust. Speech Signal Processing*, vol. 38, pp. 814–824, 1990.

[14] A. J. van der Veen, E. F. Deprettere, and A. L. Swindlehurst, "Subspace based signal analysis using singular value decomposition," *Proc. IEEE*, vol. 81, pp. 1277–1308, 1993.

[15] Y. Hua and T. K. Sarkar, "On SVD for estimating generalized eigenvalues of singular matrix pencils in noise," *IEEE Trans. Signal Processing*, vol. 39, pp. 892–900, 1991.

[16] P. Stoica and T. Soderstrom, "Statistical analysis of MUSIC and subspace rotation estimates of sinusoidal frequencies," *IEEE Trans. Signal Processing*, vol. 39, pp. 1836–1847, 1991.

[17] R. Roy and T. Kailath, "ESPRIT—Estimation of signal parameters via rotational invariance techniques," *IEEE Trans. Acoust. Speech Signal Processing*, vol. 37, pp. 984–995, 1989.

[18] A. C. H. Yu, "Eigen-based signal processing methods for ultrasound color flow imaging," Ph.D. dissertation, University of Toronto, Toronto, ON, Canada, 2007.

[19] G. H. Golub and C. F. van Loan, *Matrix Computations*. 3rd ed. Baltimore, MD: Johns Hopkins University Press, 1996.

[20] L. Y. L. Mo, T. L. Ji, C. H. Chou, D. Napolitano, G. W. McLaughlin, and D. DeBusschere, "Zone-based color flow imaging," in *Proc. IEEE Ultrason. Symp.*, 2003, pp. 29–32.

[21] D. W. Tufts and R. Kumaresan, "Estimation of frequencies of multiple sinusoids: Making linear prediction perform like maximum likelihood," *Proc. IEEE*, vol. 70, pp. 975–989, 1982.
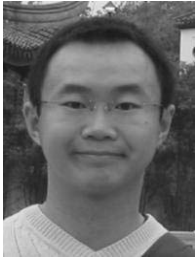
**Alfred C. H. Yu** (S'99–M'07) was born in Hong Kong in 1980. He received his B.Sc. degree in electrical engineering from the University of Calgary, AB, Canada, in 2002. He then completed his M.A.Sc. and Ph.D. degrees in electrical engineering (biomedical stream) from the University of Toronto, ON, Canada, in 2003 and 2006, respectively. In the summer of 2005, he was a research intern at Philips Research, Briarcliff Manor, NY, United States.

For his graduate work, Alfred studied the theoretical aspects of eigen-based signal processing strategies for Doppler ultrasound and color-flow imaging. He also worked on the modeling of Doppler ultrasound signals and Doppler spectral broadening. His graduate work was funded by the Canada Graduate Scholarship program from the Natural Sciences and Engineering Research Council of Canada.

Alfred is currently a postdoctoral research fellow and honorary assistant professor in the Department of Electrical and Electronic Engineering at the University of Hong Kong. His research interests are broadly centered around the design aspects of ultrasound systems and devices. He is also interested in studying the fundamentals and physics of ultrasound.

**Richard S. C. Cobbold** (M'59–LM'96) received the B.Sc. degree in physics from Imperial College, University of London in 1956, and obtained the M.Sc. and Ph.D. degrees from the University of Saskatchewan, Canada in 1961 and 1965, respectively. Since 1966, he has been with the Institute of Biomaterials and Biomedical Engineering, University of Toronto, where he was director from 1974 through to 1983. He is currently professor emeritus in the institute and in the Department of Electrical and Computer Engineering. His research interests center around the fundamental aspects of ultrasound, Doppler ultrasound, and its application for vascular assessment. He is the author of three graduate-level books, a number of research papers, and several book chapters. His most recent book, *Foundations of Biomedical Ultrasound*, was published by Oxford University Press in 2006. He was elected a Fellow of the Royal Society of Canada in 1976 and was appointed Canada-UK Rutherford lecturer in 1995.